KSME Journal, Vol. 9, No. 2, pp. 225~239, 1995

Effects of Axial Temperature Gradient on Momentum and Heat Transfer with Oscillating Pressure and Flow

Eun Soo Jeong*

(*Received August 20, 1994*)

Effects of axial temperature gradient on heat transfer, momentum transfer and energy conversion mechanisms within a closed cylinder-piston apparatus are analyzed. Assuming that the gas density change is small, the first-order and steady second-order solutions of continuity, momentum and energy equations are obtained. The solutions show that there exists a steady circulating flow and the magnitude of the steady axial velocity increases as the axial temperature gradient increases. There exists not only an oscillating component of heat flux between the gas and the wall, but also a steady component whose direction depends on axial temperature gradient. It is shown that heat is pumped from the wall near the piston to the wall near closed-end for negative axial temperature gradient. Heat transfer relation for both oscillating pressure and oscillating flow conditions is proposed.

Key Words: Oscillating Pressure, Oscillating Flow, Heat Transfer, Secondary Flow, Axial Temperature Gradient, Surface Heat Pumping, Hysteresis Loss

Nomenclature

a_0 : Speed of sound $=\sqrt{\gamma RT}$
C_p : Specific heat for constant pressure
H : Half the distance between the parallel plates (Fig. 1)
i : Imaginary unit $=\sqrt{-1}$
k : Thermal conductivity
L : Mean distance between the closed end and the piston (Fig. 1)
Ma : Mach number $=\omega s/\sqrt{\gamma RT_m}$
Nu_c : Complex Nusselt number
p : Pressure
Pr : Prandtl number $=\nu/\alpha$
q_s : Steady heat flux from the gas to the wall
R : Gas constant
$\Re$: Real part of a complex variable or number
s : Amplitude of piston motion
T : Temperature
T_{bulk} : Bulk temperature of gas
t : Time
u : Velocity component parallel to the wall
v : Velocity component perpendicular to the wall
x, y : Cartesian coordinates (Fig. 1)
α : Thermal diffusivity $=k/\rho C_p$
β : Parameter defined in Eq. (24)
γ : Specific heat ratio
ζ : Parameter defined in Eq. (40)
η : Dimensionless distance from the wall defined in Eq. (29)
λ_r : Parameter defined in Eq. (25)
λ_i : Parameter defined in Eq. (26)
μ : Shear viscosity
ν : Kinematic viscosity $=\mu/\rho$
ρ : Density
τ : Period of a cycle
ω : Angular frequency, Vorticity

Subscripts

0 : Zeroth-order value or variable, mean variable
1 : First-order value or variable
2 : Second-order value or variable
i : Imaginary part of a complex number or variable
m : Mean value defined at T_m

* Department of Mechanical Engineering, Hong-Ik University, 72-1 Sangsudong, Mapo-ku, Seoul, 121-791, Korea

r : Real part of a complex number or variable
s : Steady component of the second-order solution
w : Value at the wall

1. Introduction

The working spaces of many energy conversion systems such as Stirling machines, internal combustion engines, cryocoolers and gas springs operate under conditions of oscillating pressure and/or oscillating flow. The heat transfer associated with these conditions has a strong effect on the system's performance(Tew, 1987), and the heat transfer rate at the wall cannot be predicted by the heat transfer correlations developed for steady pressure and steady flow(Pfriem, 1943; Annand and Pinfold, 1980; Lee, 1983; Faulkner and Smith, 1983; Kornhauser and Smith, 1988a and 1988b; Jeong and Smith, 1992a and 1992b). Moreover, the working gases of pulse tube refrigerators and thermoacoustic engines/refrigerators, which operate under conditions of oscillating pressure and oscillating flow, are in contact with cylinder wall with non-zero axial temperature gradient. Due to the phase difference between pressure and temperature caused by heat transfer between the gas and the wall, each element of the gas undergoes a thermodynamic cycle as it oscillates within the working space. There exists a critical axial temperature gradient which is the boundary between heat pump and prime mover functions of thermoacoustic engines(Swift, 1988). Gifford and Longsworth(1963) devised a pulse tube refrigerator and experimentally showed cooling from the colder wall near oscillating piston and heating of the hotter wall near closed end. They named this phenomenon 'surface heat pumping' effect and qualitatively explained its mechanism(Gifford and Longsworth, 1966).

Previous theoretical investigations(Lee, 1983; Merkli and Thomann, 1975; Jeong and Smith, 1992a and 1992b) considered heat transfer and related phenomena under oscillating pressure and/or oscillating flow with zero axial wall temperature gradient. Pfriem(1943) and Lee(1983) proposed one-dimensional heat conduction models for engine heat transfer and closed reciprocating engine heat transfer, respectively. Convection and density variation were assumed to be negligible. Pfriem first proposed the use of a complex heat transfer coefficient for oscillating pressure conditions. Lee's model predicted heat transfer and hysteresis loss fairly well for small density variation(Kornhauser and Smith, 1988a and 1988b). Jeong and Smith(1992a) analyzed momentum and heat transfers in a closed-volume cylinder-piston apparatus and showed that there exists a steady circulating flow due to the density gradient in the direction normal to the wall and the interaction of inertia and viscosity. Their results successfully explained unanswered questions, raised from previous experiments, such as suppression of correlation breakdown regions by fins and Mach number effect on hysteresis loss and complex Nusselt number(Faulkner and Smith, 1983 and 1984; Kornhauser and Smith, 1988a and 1988b). Jeong and Smith(1992b) also proposed an analytic model which has no limitation on the density variation of the gas. The predictions of this model were in good agreement with experiments and showed that the compression ratio is an important independent parameter. Merkli and Thomann(1975) observed slight cooling around the pressure node and heating around the pressure antinode of resonance tube, and presented an analytic theory for this effect. They also observed steady secondary weak vortices along the tube wall, which seem to confirm the existence of large scale circulation. Recently, Lee et al.(1993) observed large scale streaming for both basic pulse tube and orifice pulse tube refrigerator configurations.

In this paper, momentum and heat transfers in a closed-volume cylinder-piston apparatus with non-zero axial temperature gradient are analyzed. Continuity, momentum and energy equations as well as equation of state for the working gas in a cylinder-piston apparatus are solved. In addition to the first-order solution which is periodic in time, the steady component of the second-order solution is obtained. Based on these solutions effects of axial wall temperature gradient on heat and momentum transfer and other related phe-

nomena are discussed.

2. Analysis

Our attention will be restricted to the gas between the parallel plates with one end closed and the other end equipped by a piston as shown in Fig. 1. The plates have constant axial temperature gradient in the x-direction dT_m/dx. The gas is compressed and expanded by sinusoidal motion of the piston. Although most of the working spaces of actual reciprocating machines have a shape of circular cylinder, parallel plates were chosen here to simplify the analysis. The fundamental results for parallel plates are likely to be similar to those for circular cylinders when the important phenomena take place in a relatively thin boundary layer.

The main assumption of the analysis is that the heat conduction and the velocity gradient in the x-direction are negligible compared to those in the y-direction. The choice of parallel plates instead of circular cylinder and the assumption of negligible heat conduction and velocity gradient in the x-direction are appropriate for most reciprocating machines such as Stirling engines and pulse tube refrigerators since momentum and thermal boundary layer thicknesses are far thinner than cylinder diameter. We also assume that the temperatures of the plates do not vary with time since the heat capacities of the cylinder wall for reciprocating machines are far larger than that of the gas. Under additional assumptions of laminar flow, perfect gas, constant physical properties and negligible body force, which are appropriate for pulse tube refrigerators and thermoacoustic engines/refrigerators, especially, the conservation laws of mass, momentum and energy as well as the equation of state can be written as follows (in two-dimensional Cartesian coordinates):

$$\frac{\partial \rho}{\partial t}+\frac{\partial(\rho u)}{\partial x}+\frac{\partial(\rho v)}{\partial y}=0 \tag{1}$$

$$\rho\left(\frac{\partial u}{\partial t}+u\frac{\partial u}{\partial x}+v\frac{\partial u}{\partial y}\right)=-\frac{\partial p}{\partial x}+\mu\frac{\partial^2 u}{\partial y^2} \tag{2}$$

$$\frac{\partial p}{\partial y}=0 \tag{3}$$

$$\rho C_p\left(\frac{\partial T}{\partial t}+u\frac{\partial T}{\partial x}+v\frac{\partial T}{\partial y}\right)+\rho\left\{\frac{\partial}{\partial t}\left(\frac{u^2+v^2}{2}\right)+u\frac{\partial}{\partial x}\left(\frac{u^2+v^2}{2}\right)+v\frac{\partial}{\partial y}\left(\frac{u^2+v^2}{2}\right)\right\}=k\frac{\partial^2 T}{\partial y^2}+\frac{\partial p}{\partial t}-\mu u\frac{\partial^2 u}{\partial y^2}-\mu\left(\frac{\partial u}{\partial y}\right)^2 \tag{4}$$

$$p=\rho RT \tag{5}$$

The boundary conditions for the system configuration in Fig. 1 are given as follows:

$y=0$:

$u=0,\ v=0,$

$T=T_w(x)=T_m+(dT_m/dx)x$

$y=H$:

$\frac{\partial u}{\partial y}=0,\ \frac{\partial T}{\partial y}=0,\ v=0$

$x=0$:

$u=0$

$x=L+s\sin(\omega t)$:

$u=\omega s\cos(\omega t)$ (6)

The governing Eqs. (1)~(5) are integrated by the method of successive approximations (Schlichting, 1979, p. 410; Merkli and Thomann, 1975; Jeong, 1991) with the assumption of small amplitude of piston motion, i. e., $s/L\ll 1$. This assumption is appropriate for pulse tube refrigerators and thermoacoustic engines/refrigerators

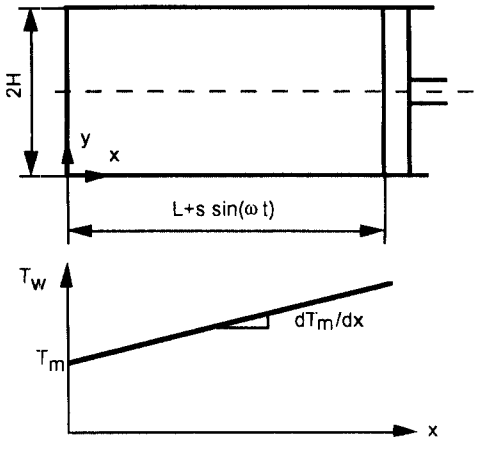

Fig. 1 Schematic diagram of a cylinder-piston apparatus and wall temperature profile

where stroke of the piston is far shorter than the length of the machines. In this method all unknowns are expressed as a sum of zeroth-order term plus higher-order terms:

$$\begin{aligned}\rho&=\rho_0+\rho_1+\rho_2+\cdots\\ u&=0+u_1+u_2+\cdots\\ v&=0+v_1+v_2+\cdots\\ T&=T_0+T_1+T_2+\cdots\\ p&=p_0+p_1+p_2+\cdots\end{aligned}\tag{7}$$

A product of two first-order terms is assumed to be a second-order term, while a product of a zeroth-order term with a first-order or a second-order term still remains a first-order or a second-order term.

Substituting the expressions of Eq. (7) into Eqs. (1)~(5) and keeping only the first-order terms, with further assumptions of $(dT_m/dx)L/T_m\ll 1$ and that the zeroth-order temperature T_0 is independent of y and is the same as that of the plate, we can obtain the following first-order equations.

$$\frac{\partial\rho_1}{\partial t}+\rho_0\frac{\partial u_1}{\partial x}+\rho_0\frac{\partial v_1}{\partial y}=0 \tag{8}$$

$$\rho_0\frac{\partial u_1}{\partial t}=-\frac{\partial p_1}{\partial x}+\mu\frac{\partial^2 u_1}{\partial y^2} \tag{9}$$

$$\frac{\partial p_1}{\partial y}=0 \tag{10}$$

$$\rho_0 C_p\left(\frac{\partial T_1}{\partial t}+u_1\frac{dT_m}{dx}\right)=k\frac{\partial^2 T_1}{\partial y^2}+\frac{\partial p_1}{\partial t} \tag{11}$$

$$p_1=\rho_0 RT_1+\rho_1 RT_0 \tag{12}$$

Keeping only the second-order terms, second-order equations are obtained as follows.

$$\frac{\partial\rho_2}{\partial t}+\rho_0\frac{\partial u_2}{\partial x}+\rho_0\frac{\partial v_2}{\partial y}=-\frac{\partial(\rho_1 u_1)}{\partial x}-\frac{\partial(\rho_1 v_1)}{\partial y} \tag{13}$$

$$\rho_0\frac{\partial u_2}{\partial t}+\frac{\partial p_2}{\partial x}-\mu\frac{\partial^2 u_2}{\partial y^2}=-\rho_0 u_1\frac{\partial u_1}{\partial x}-\rho_0 v_1\frac{\partial u_1}{\partial y}-\rho_1\frac{\partial u_1}{\partial t} \tag{14}$$

$$\frac{\partial p_2}{\partial y}=0 \tag{15}$$

$$\begin{aligned}\rho_0 C_p\frac{\partial T_2}{\partial t}-k\frac{\partial^2 T_2}{\partial y^2}-\frac{\partial p_2}{\partial t}=&-\rho_1 C_p\frac{\partial T_1}{\partial t}-\rho_0 C_p u_1\frac{\partial T_1}{\partial x}-\rho_0 C_p v_1\frac{\partial T_1}{\partial y}-\rho_0\frac{\partial}{\partial t}\left(\frac{u_1^2+v_1^2}{2}\right)\\ &-\mu u_1\frac{\partial^2 u_1}{\partial y^2}-\mu\left(\frac{\partial u_1}{\partial y}\right)^2-\rho_1 C_p u_1\frac{dT_m}{dx}-\rho_0 C_p u_2\frac{dT_m}{dx}\end{aligned} \tag{16}$$

$$p_2=\rho_0 RT_2+\rho_2 RT_0+\rho_1 RT_1 \tag{17}$$

The boundary conditions of the first-order Eqs. (8) to (12) are $u_1=v_1=T_1=0$ at $y=0$, $\partial u_1/\partial y=\partial T_1/\partial y=v_1=0$ at $y=H$, $u_1=0$ at $x=0$ and $u_1=\omega s\cos(\omega t)$ at $x=L$. Since the boundary condition at $x=L$ cannot be satisfied exactly, the boundary condition at the piston surface is satisfied in cross-sectional average sense(Merkli and Thomann, 1975; Jeong, 1991).

$$\int_0^H u_1(x=L,\ y)dy=\omega sH\cos(\omega t) \tag{18}$$

Since the first-order solution is purely periodic in time, the unknowns can be expressed as $u_1=\hat{u}_1(x,\ y)e^{i\omega t}$, $v_1=\hat{v}_1(x,\ y)e^{i\omega t}$, $T_1=\hat{T}_1(x,\ y)e^{i\omega t}$, $\rho_1=\hat{\rho}_1(x,\ y)e^{i\omega t}$, $p_1=\hat{p}_1(x,\ y)e^{i\omega t}$. After substituting these expressions into Eqs. (8) to (12) we can get $\hat{u}_1$, $\hat{T}_1$, $\hat{p}_1$ from Eqs. (9), (11) and (12) in terms of $\hat{p}_1$. $\hat{v}_1$ and $\hat{p}_1$ can be obtained from Eqs. (8) and (18). The solution of the first-order equations is given as follows. Only the real parts of the complex quantities have physical meaning.

$$u_1(x,\ y,\ t)=\frac{i}{\rho_m\omega}\frac{dp_1}{dx}\left\{1-\frac{\cosh[(1+i)\beta(1-y/H)]}{\cosh[(1+i)\beta]}\right\} \tag{19}$$

$$\begin{aligned}v_1(x,\ y,\ t)=&\frac{iH}{\rho_m\omega}\frac{d^2p_1}{dx^2}\left[-\frac{y}{H}+\frac{1}{(1+i)\beta}\left\{\tanh[(1+i)\beta]-\frac{\sinh[(1+i)\beta(1-y/H)]}{\cosh[(1+i)\beta]}\right\}\right]\\ &+\frac{i\omega H}{\gamma\rho_m RT_m}p_1\left[-\frac{y}{H}-\frac{(\gamma-1)}{(1+i)\beta\sqrt{Pr}}\left\{\tanh[(1+i)\beta\sqrt{Pr}]\right.\right.\\ &\left.\left.-\frac{\sinh[(1+i)\beta\sqrt{Pr}(1-y/H)]}{\cosh[(1+i)\beta\sqrt{Pr}]}\right\}\right]\end{aligned}$$

$$+\frac{iH}{\rho_m\omega T_m}\frac{dT_m}{dx}\frac{dp_1}{dx}\left[-\frac{y}{H}+\frac{Pr}{Pr-1}\frac{1}{(1+i)\beta}\left\{\tanh[(1+i)\beta]-\frac{\sinh[(1+i)\beta(1-y/H)]}{\cosh[(1+i)\beta]}\right\}\right.$$
$$\left.-\frac{1}{Pr-1}\frac{1}{(1+i)\beta\sqrt{Pr}}\left\{\tanh[(1+i)\beta\sqrt{Pr}]-\frac{\sinh[(1+i)\beta\sqrt{Pr}(1-y/H)]}{\cosh[(1+i)\beta\sqrt{Pr}]}\right\}\right] \tag{20}$$

$$T_1(x,\ y,\ t)=\frac{P_1}{\rho_m C_p}\left\{1-\frac{\cosh[(1+i)\beta\sqrt{Pr}(1-y/H)]}{\cosh[(1+i)\beta\sqrt{Pr}]}\right\}$$
$$-\frac{1}{\rho_m\omega^2}\frac{dT_m}{dx}\frac{dp_1}{dx}\left\{1-\frac{Pr}{Pr-1}\frac{\cosh[(1+i)\beta(1-y/H)]}{\cosh[(1+i)\beta]}\right.$$
$$\left.+\frac{1}{Pr-1}\frac{\cosh[(1+i)\beta\sqrt{Pr}(1-y/H)]}{\cosh[(1+i)\beta\sqrt{Pr}]}\right\} \tag{21}$$

$$\rho_1(x,\ y,\ t)=\frac{p_1}{\gamma RT_m}\left\{1+(\gamma-1)\frac{\cosh[(1+i)\beta\sqrt{Pr}(1-y/H)]}{\cosh[(1+i)\beta\sqrt{Pr}]}\right\}$$
$$+\frac{1}{\omega^2 T_m}\frac{dT_m}{dx}\frac{dp_1}{dx}\left\{1-\frac{Pr}{Pr-1}\frac{\cosh[(1+i)\beta(1-y/H)]}{\cosh[(1+i)\beta]}\right.$$
$$\left.+\frac{1}{Pr-1}\frac{\cosh[(1+i)\beta\sqrt{Pr}(1-y/H)]}{\cosh[(1+i)\beta\sqrt{Pr}]}\right\} \tag{22}$$

$$p_1(x,\ t)=\frac{i\gamma\rho_m RT_m S}{D(\beta)}e^{\lambda_r(L-x)}$$
$$\frac{(\lambda_i\cos\lambda_i x+\lambda_r\sin\lambda_i x)}{\sin\lambda_i L}\frac{1}{\{1-\tanh[(1+i)\beta]/[(1+i)\beta]\}}e^{i\omega t} \tag{23}$$

where

$$\beta=H/\sqrt{2\nu_0/\omega} \tag{24}$$

$$\lambda_r=\frac{C(\beta)}{2}\frac{(dT_m/dx)}{T_m} \tag{25}$$

$$\lambda_i=\sqrt{D(\beta)\frac{\omega^2}{\gamma RT_m}-\left(\frac{C(\beta)}{2}\frac{(dT_m/dx)}{T_m}\right)^2} \tag{26}$$

$$C(\beta)=\frac{1-\frac{Pr}{Pr-1}\frac{\tanh[(1+i)\beta]}{(1+i)\beta}+\frac{1}{Pr-1}\frac{\tanh[(1+i)\beta\sqrt{Pr}]}{(1+i)\beta\sqrt{Pr}}}{1-\frac{\tanh[(1+i)\beta]}{(1+i)\beta}} \tag{27}$$

$$D(\beta)=\frac{1+(\gamma-1)\frac{\tanh[(1+i)\beta\sqrt{Pr}]}{(1+i)\beta\sqrt{Pr}}}{1-\frac{\tanh[(1+i)\beta]}{(1+i)\beta}} \tag{28}$$

Gas motion between the parallel plates induced by harmonic oscillation of a flat piston is well described by this solution as long as the frequency is below the resonant frequency and the boundary layer thickness is small compared with the width between the plates, $2H$(i. e., $\beta>1$). In the pulse tube of basic type pulse tube refrigerators and in the stack of thermoacoustic engines/refrigerators momentum and thermal boundary layer thicknesses are comparable with the cylinder radius(i. e., $\beta\sim1$). For other reciprocating machines the boundary layer thicknesses are far thinner than cylinder radius(i. e., $\beta\gg1$). The first-order solution is purely oscillatory in time. Thus, heat flux obtained from the first-order solution cannot explain the surface heat pumping effect(Gifford and Longsworth, 1963 and 1966) and how the net work done by the piston on the gas is removed from the gas to the wall as heat for the gas to maintain cyclic steady state(Jeong, 1991 ; Jeong and Smith, 1992a). Since only terms of second-order and higher-order in the energy equation contribute to a time-independent heat flux, we have to obtain the second-order solutions. The

solution of the second-order equations consists of unsteady terms with frequency 2ω and steady terms, i. e., time-independent terms. Since we are interested in the time-averaged behavior, only the steady component of the second-order solution is obtained. We also restrict our attention to the case of thin boundary layer. For $\beta \gg 1$ the first-order solution, λ_r and λ_i are simplified as follows.

$$u_1=\omega s e^{\lambda_r(L-x)}\frac{\sin\lambda_i x}{\sin\lambda_i L}\{\cos\omega t-e^{-\eta}\cos(\omega t-\eta)\} \tag{19'}$$

$$\begin{aligned} v_1=&\frac{\omega sH\lambda_i}{\sqrt{2}\beta}e^{\lambda_r(L-x)}\\ &\frac{\cos\lambda_i x+(\lambda_r/\lambda_i)\sin\lambda_i x}{\sin\lambda_i L}\left\{\left(1+\frac{\gamma-1}{\sqrt{Pr}}\right)\left(1-\frac{\eta}{\beta}\right)\cos\left(\omega t-\frac{\pi}{4}\right)-e^{-\eta}\cos\left(\omega t-\eta-\frac{\pi}{4}\right)\right.\\ &\left.-\frac{\gamma-1}{\sqrt{Pr}}e^{-\sqrt{Pr}\,\eta}\cos\left(\omega t-\sqrt{Pr}\,\eta-\frac{\pi}{4}\right)\right\}\\ &+\frac{\omega sH}{\sqrt{2(Pr-1)}\beta}\frac{(dT_m/dx)}{T_m}e^{\lambda_r(L-x)}\frac{\sin\lambda_i x}{\sin\lambda_i L}\left\{\left(1-\frac{1}{\sqrt{Pr}}\right)\left(1-\frac{\eta}{\beta}\right)\cos\left(\omega t-\frac{\pi}{4}\right)\right.\\ &\left.-e^{-\eta}\cos\left(\omega t-\eta-\frac{\pi}{4}\right)+\frac{1}{\sqrt{Pr}}e^{-\sqrt{Pr}\,\eta}\cos\left(\omega t-\sqrt{Pr}\,\eta-\frac{\pi}{4}\right)\right\} \end{aligned} \tag{20'}$$

$$\begin{aligned} T_1=&-(\gamma-1)T_m s\lambda_i e^{\lambda_r(L-x)}\frac{\cos\lambda_i x+(\lambda_r/\lambda_i)\sin\lambda_i x}{\sin\lambda_i L}\{\sin\omega t-e^{-\sqrt{Pr}\,\eta}\sin(\omega t-\sqrt{Pr}\,\eta)\}\\ &-\frac{dT_m}{dx}se^{\lambda_r(L-x)}\frac{\sin\lambda_i x}{\sin\lambda_i L}\left\{\sin\omega t-\frac{Pr}{Pr-1}e^{-\eta}\sin(\omega t-\eta)\right.\\ &\left.+\frac{1}{Pr-1}e^{-\sqrt{Pr}\,\eta}\sin(\omega t-\sqrt{Pr}\,\eta)\right\} \end{aligned} \tag{21'}$$

$$\begin{aligned} \rho_1=&\rho_m s\lambda_i e^{\lambda_r(L-x)}\frac{\cos\lambda_i x+(\lambda_r/\lambda_i)\sin\lambda_i x}{\sin\lambda_i L}\{-\sin\omega t-(\gamma-1)e^{-\sqrt{Pr}\,\eta}\sin(\omega t-\sqrt{Pr}\,\eta)\}\\ &+\rho_m\frac{(dT_m/dx)}{T_m}se^{\lambda_r(L-x)}\frac{\sin\lambda_i x}{\sin\lambda_i L}\left\{\sin\omega t-\frac{Pr}{Pr-1}e^{-\eta}\sin(\omega t-\eta)\right.\\ &\left.+\frac{1}{Pr-1}e^{-\sqrt{Pr}\,\eta}\sin(\omega t-\sqrt{Pr}\,\eta)\right\} \end{aligned} \tag{22'}$$

$$p_1=-\gamma\rho_m RT_m s\lambda_i e^{\lambda_r(L-x)}\frac{\cos\lambda_i x+(\lambda_r/\lambda_i)\sin\lambda_i x}{\sin\lambda_i L}\sin\omega t \tag{23'}$$

where

$$\lambda_r\cong-\frac{(dT_m/dx)}{2T_m} \tag{25'}$$

$$\lambda_i\cong\sqrt{\frac{\omega^2}{\gamma RT_m}-\left(\frac{dT_m/dx}{2T_m}\right)^2} \tag{26'}$$

$$\eta\equiv\beta\frac{y}{H}=\frac{y}{\sqrt{2\nu_0/\omega}} \tag{29}$$

Substituting Eqs. (19′)~(23′) into the time-averaged second-order momentum and energy equations obtained from Eqs. (14) and (16) and integrating twice with respect to y, the steady components of x-direction velocity and temperature are given as follows. Boundary conditions $T_s=0$ at $y=0$, $\partial T_s/\partial y=0$ at $y=H$, $u_s=0$ at $y=0$, $\partial u_s/\partial y=0$ at $y=H$, and the time-averaged mass balance across any cross-section, which can be obtained from Eq. (13) are used.

$$\int_0^H[\rho_0 u_s+<\rho_1 u_1>]dy=0 \tag{30}$$

Here u_s is the steady component of u_2 and angular bracket ($<>$) denotes time averaging.

$$u_s=\frac{1}{2}\omega s\frac{s}{L}e^{2\lambda_r(L-x)}\frac{\sin\lambda_i x(-\lambda_r L\sin\lambda_i x+\lambda_i L\cos\lambda_i x)}{\sin^2\lambda_i L}\left[-\frac{1}{2}+\frac{3}{4}\left\{2\frac{\eta}{\beta}-\left(\frac{\eta}{\beta}\right)^2\right\}+2e^{-\eta}\sin\eta\right.$$

$$+\frac{1}{2}e^{-2\eta}\Big]+\frac{1}{2}\omega s\frac{s}{L}e^{2\lambda_r(L-x)}\frac{\sin\lambda_i x(\lambda_i L\cos\lambda_i x+\lambda_r L\sin\lambda_i x)}{\sin^2\lambda_i L}\Big[\Big(1+\frac{(\gamma-1)\sqrt{Pr}}{1+Pr}\Big)\Big\{-1+3\frac{\eta}{\beta}$$

$$-\frac{3}{2}\Big(\frac{\eta}{\beta}\Big)^2\Big\}+\Big(1+\frac{\gamma-1}{\sqrt{Pr}}\Big)\frac{1}{\beta}+\Big\{1+\Big(1+\frac{\gamma-1}{\sqrt{Pr}}\Big)\frac{1}{\beta}\Big\}e^{-\eta}\sin\eta+\Big(1+\frac{\gamma-1}{\sqrt{Pr}}\Big)\Big(1-\frac{\eta+1}{\beta}\Big)e^{-\eta}\cos\eta$$

$$-\frac{\gamma-1}{Pr}e^{-\sqrt{Pr}\,\eta}\sin\sqrt{Pr}\,\eta-\frac{\gamma-1}{(1+Pr)\sqrt{Pr}}e^{-(1+\sqrt{Pr})\eta}\{\sqrt{Pr}\sin(1-\sqrt{Pr})\eta+\cos(1-\sqrt{Pr})\eta\}]$$

$$+\frac{1}{2}\omega s\frac{s}{L}\frac{(dT_m/dx)}{T_m/L}e^{2\lambda_r(L-x)}\Big(\frac{\sin\lambda_i x}{\sin\lambda_i L}\Big)^2\Big[\frac{Pr^2+Pr\sqrt{Pr}+2\sqrt{Pr}-2}{2\sqrt{Pr}(1+\sqrt{Pr})(1+Pr)}\Big\{1-3\frac{\eta}{\beta}+\frac{3}{2}\Big(\frac{\eta}{\beta}\Big)^2\Big\}$$

$$+\frac{1}{\beta(1+\sqrt{Pr})\sqrt{Pr}}-\frac{Pr}{2(Pr-1)}e^{-2\eta}-\Big(\frac{2Pr-1}{Pr-1}-\frac{1}{(1+\sqrt{Pr})\sqrt{Pr}\,\beta}\Big)e^{-\eta}\sin\eta$$

$$+\frac{1}{(1+\sqrt{Pr})\sqrt{Pr}}\Big(1-\frac{\eta+1}{\beta}\Big)e^{-\eta}\cos\eta+\frac{1}{(Pr-1)Pr}e^{-\sqrt{Pr}\,\eta}\sin\sqrt{Pr}\,\eta$$

$$-\frac{1}{(Pr^2-1)\sqrt{Pr}}e^{-(1+\sqrt{Pr})\eta}\{\sin(1-\sqrt{Pr})\eta-\sqrt{Pr}\cos(1-\sqrt{Pr})\eta\}] \tag{31}$$

$$T_s=T_m Pr(\gamma-1)\Big(\frac{s}{L}\Big)^2e^{2\lambda_r(L-x)}\Big(\frac{\lambda_i L\cos\lambda_i x+\lambda_r L\sin\lambda_i x}{\sin\lambda_i L}\Big)^2\Big[\frac{\gamma-1}{4Pr}(e^{-2\sqrt{Pr}\,\eta}-1)$$

$$+\frac{\gamma+\sqrt{Pr}-1}{2Pr}\Big(1-\frac{1}{\beta}\Big(\eta+\frac{1}{\sqrt{Pr}}\Big)\Big)e^{-\sqrt{Pr}\,\eta}\sin\sqrt{Pr}\,\eta+\frac{1}{2Pr}\Big(\gamma+\frac{\gamma+\sqrt{Pr}-1}{\sqrt{Pr}\,\beta}\Big)\cdot$$

$$(1-e^{-\sqrt{Pr}\,\eta}\cos\sqrt{Pr}\,\eta)+\frac{\sqrt{Pr}}{2(1+Pr)^2}\{-(1-Pr)e^{-(1+\sqrt{Pr})\eta}\sin(1-\sqrt{Pr})\eta$$

$$+2\sqrt{Pr}\,(e^{-(1+\sqrt{Pr})\eta}\cos(1-\sqrt{Pr})\eta-1)\}\Big]$$

$$+Pr\Big(\frac{s}{L}\Big)^2L\frac{dT_m}{dx}e^{2\lambda_r(L-x)}\frac{\sin\lambda_i x(\lambda_i L\cos\lambda_i x+\lambda_r L\sin\lambda_i x)}{\sin^2\lambda_i L}\Big[\frac{Pr}{4(Pr-1)}(e^{-2\eta}-1)$$

$$+\frac{\gamma-1}{2Pr(Pr-1)}(1-e^{-2\sqrt{Pr}\,\eta})+\Big(1+\frac{\gamma-1}{\sqrt{Pr}}\Big)\Big(\frac{\eta^2}{2\beta}-\eta\Big)+\Big(1+\frac{(\gamma-1)\sqrt{Pr}}{1+Pr}\Big)\cdot$$

$$\Big(-\frac{\eta^2}{2}+\frac{\eta^3}{2\beta}-\frac{\eta^4}{8\beta^2}\Big)+\frac{1}{2(Pr-1)}\Big(1+\frac{\gamma-1}{\sqrt{Pr}}\Big)\Big(1-\frac{2-Pr+\eta}{\beta}\Big)e^{-\eta}\sin\eta$$

$$+\Big(1-\frac{\gamma Pr}{2(Pr-1)}-\frac{2-Pr}{2(Pr-1)}\Big(1+\frac{\gamma-1}{\sqrt{Pr}}\Big)\frac{1}{\beta}\Big)(e^{-\eta}\cos\eta-1)$$

$$+\frac{(\gamma-1)(\sqrt{Pr}-2)-\sqrt{Pr}}{2Pr(Pr-1)}\Big\{1-\frac{1}{\beta}\Big(\eta+\frac{1}{\sqrt{Pr}}\Big)\Big\}e^{-\sqrt{Pr}\,\eta}\sin\sqrt{Pr}\,\eta$$

$$+\frac{1}{2Pr}\Big\{\frac{\gamma}{Pr-1}+\frac{(\gamma-1)(Pr-1)}{Pr}-\frac{(\gamma-1)(\sqrt{Pr}-2)-\sqrt{Pr}}{\sqrt{Pr}(Pr-1)}\frac{1}{\beta}\Big\}(e^{-\sqrt{Pr}\,\eta}\cos\sqrt{Pr}\,\eta-1)$$

$$+\frac{1}{2(1+Pr)^2}\Big\{\Big(\frac{(\gamma-1)(2Pr^2-Pr+1)}{(1+Pr)\sqrt{Pr}}-\sqrt{Pr}(3-2\gamma)\Big)e^{-(1+\sqrt{Pr})\eta}\sin(1-\sqrt{Pr})\eta$$

$$+\Big(\frac{(\gamma-1)(Pr^2-Pr+2)}{1+Pr}+\frac{2(3-2\gamma)Pr}{Pr-1}\Big)(1-e^{-(1+\sqrt{Pr})\eta}\cos(1-\sqrt{Pr})\eta)\Big\}\Big]+T_m Pr(\gamma-1)\cdot$$

$$Ma^2e^{2\lambda_r(L-x)}\Big(\frac{\sin\lambda_i x}{\sin\lambda_i L}\Big)^2\Big[\frac{3}{4}+\frac{1}{4}e^{-2\eta}-e^{-\eta}\cos\eta-\frac{1}{2Pr}(1-e^{-\sqrt{Pr}\,\eta}\cos\sqrt{Pr}\,\eta)$$

$$+\frac{1}{2(1+Pr)^2}\Big\{2\sqrt{Pr}\,e^{-(1+\sqrt{Pr})\eta}\sin(1-\sqrt{Pr})\eta+(1-Pr)\Big(e^{-(1+\sqrt{Pr})\eta}\cos(1-\sqrt{Pr})\eta-1\Big)\Big\}\Big]$$

$$+Pr\Big(\frac{s}{L}\Big)^2L\frac{dT_m}{dx}e^{2\lambda_r(L-x)}\frac{\sin\lambda_i x(-\lambda_r L\sin\lambda_i x+\lambda_i L\cos\lambda_i x)}{\sin^2\lambda_i L}\Big[-\frac{\eta^2}{4}+\frac{\eta^3}{4\beta}-\frac{\eta^4}{16\beta^2}$$

$$+\frac{1}{8}(e^{-2\eta}-1)+\frac{2Pr-3}{2(Pr-1)}(e^{-\eta}\cos\eta-1)+\frac{1}{2Pr(Pr-1)}(e^{-\sqrt{Pr}\,\eta}\cos\sqrt{Pr}\,\eta-1)$$

$$+\frac{1}{2(Pr-1)(1+Pr)^2}\{2\sqrt{Pr}\,e^{-(1+\sqrt{Pr})\eta}\sin(1-\sqrt{Pr})\eta+(1-Pr)\cdot$$

$$(e^{-(1+\sqrt{Pr})\eta}\cos(1-\sqrt{Pr})\eta-1)\}\Big]+\frac{Pr}{Pr-1}\Big(\frac{s}{L}\Big)^2\frac{(dT_m/dx)^2}{T_m/L^2}e^{2\lambda_r(L-x)}\Big(\frac{\sin\lambda_i x}{\sin\lambda_i L}\Big)^2\cdot$$

$$\left[\frac{Pr(3-Pr)}{8(Pr-1)}(e^{-2\eta}-1)-\frac{1}{4Pr(Pr-1)}(1-e^{-2\sqrt{Pr}\,\eta})+\frac{\sqrt{Pr}-1}{\sqrt{Pr}}\left(\frac{\eta^2}{2\beta}-\eta\right)\right.$$
$$+\frac{(\sqrt{Pr}-1)(Pr^2+Pr\sqrt{Pr}+2\sqrt{Pr}-2)}{2\sqrt{Pr}(1+Pr)}\left(\frac{\eta^2}{2}-\frac{\eta^3}{2\beta}+\frac{\eta^4}{8\beta^2}\right)$$
$$+\frac{1}{2\sqrt{Pr}(1+\sqrt{Pr})}\left(1-\frac{2-Pr+\eta}{\beta}\right)e^{-\eta}\sin\eta+\left(1-Pr-\frac{2-Pr}{2\sqrt{Pr}(1+\sqrt{Pr})}\frac{1}{\beta}\right)\cdot$$
$$(e^{-\eta}\cos\eta-1)-\frac{1}{2\sqrt{Pr}(1+\sqrt{Pr})}\left\{1-\frac{1}{\beta}\left(\eta+\frac{1}{\sqrt{Pr}}\right)\right\}e^{-\sqrt{Pr}\,\eta}\sin\sqrt{Pr}\,\eta$$
$$+\frac{1}{2Pr}\left\{1-\frac{1}{Pr}-\frac{1}{\sqrt{Pr}(1+\sqrt{Pr})}\frac{1}{\beta}\right\}(1-e^{-\sqrt{Pr}\,\eta}\cos\sqrt{Pr}\,\eta)$$
$$+\frac{1}{2(1+Pr)^2}\left\{\left(\frac{Pr-3}{Pr+1}-4\sqrt{Pr}\right)e^{-(1+\sqrt{Pr})\eta}\sin(1-\sqrt{Pr})\eta\right.$$
$$\left.\left.+\left(Pr+\frac{3Pr-1}{(1+Pr)\sqrt{Pr}}-\frac{5Pr-1}{Pr-1}\right)(e^{-(1+\sqrt{Pr})\eta}\cos(1-\sqrt{Pr})\eta-1)\right\}\right] \tag{32}$$

3. Results and Discussion

3.1 First-order velocity and temperature profiles

For most reciprocating machines the working fluids are air, inert gases such as helium and mixtures of inert gases. So $Pr=0.7$ and $\gamma=1.4$ were chosen here to show the behavior of working fluids. The range of Ma and s/L for most reciprocating machines are $0.001<Ma<1$ and $0<s/L<1$. $Ma\ll 1$ except thermoacoustic engines/refrigerators and $s/L\ll 1$ for pulse tube refrigerators and thermoacoustic engines/refrigerators.

The first-order axial velocity profile variation during a cycle for several values of β is shown in Fig. 2. At low values of β the velocity profiles are parabolic as in the steady state channel flow. For β of order 1($\beta=3$) boundary layer develops near the wall and the flow direction in the boundary layer is opposite to that of the core flow during parts of a cycle. At high values of β($\beta=30$) boundary layer becomes narrower and the velocity profile of the core becomes flat. The velocity takes the maximum value near the wall and the phase shift between the velocity gradient at the wall and the mean velocity becomes apparent. As can be seen from Eq. (24) the physical meaning of β is the ratio of cylinder radius to momentum boundary layer thickness. Since the boundary layer thickness decreases as the piston frequency increases, β increases as the piston frequency increases if other parameters remain constant. At low values of β the velocity profiles show the steady state channel flow profile since the piston frequency is low, but at high values of β they show very different behavior from that of the steady state channel flow.

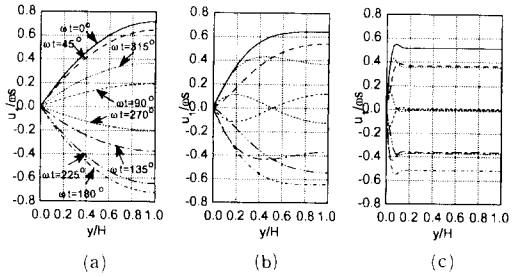

(L/s=30, Pr=0.7, γ=1.4, Ma=0.01, x/L=0.5)

Fig. 2 First-order axial velocity profiles for $(dT_m/dx)/(T_m/L)=0$

In Fig. 3 the velocity profiles in the direction normal to the wall are shown. Like the axial velocity profiles, the point of maximum velocity approaches the wall and the velocity gradient is concentrated near the wall as β increases. Also the flow direction in the boundary layer is opposite to that of the core flow during parts of a cycle for large β. The maximum velocity amplitude decreases with β.

The first-order temperature profiles for several values of β are shown in Fig. 4. For low values of β($\beta=0.3$) the temperature fluctuation is very small. For $\beta=3$ the phase shift between the temperature gradient at the wall and wall-bulk fluid

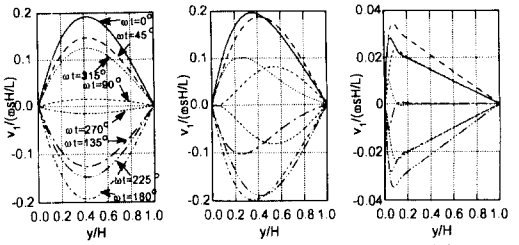

(L/s=30, Pr=0.7, γ=1.4, Ma=0.01, x/L=0.5)

Fig. 3 First-order axial velocity profiles in y-direction for $(dT_m/dx)/(T_m/L)=0$

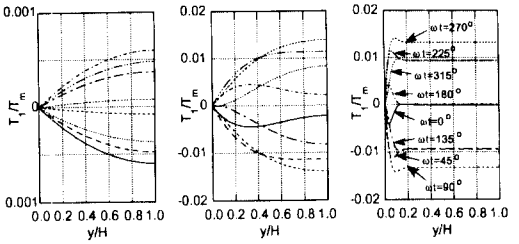

(L/s=30, Pr=0.7, γ=1.4, Ma=0.01, x/L=0.5)

Fig. 4 First-order temperature profiles for $(dT_m/dx)/(T_m/L)=0$

temperature difference begins to appear. At higher values of $\beta(\beta=30)$ thermal boundary layer becomes narrower and the temperature of the core becomes uniform.

Effect of axial temperature gradient on the first-order temperature profiles for $\beta=30$ is shown in Fig. 5. It can be seen that the amplitude of the temperature fluctuation increases as axial temperature gradient increases. As can be seen from Fig. 1 gas parcels are compressed and expanded as they oscillate within the working space by piston motion. The temperature of a gas parcel rises by compression as it moves to the left, and lowers by expansion as it moves to the right as shown in Fig. 6. When axial temperature gradient is positive, the temperature of a gas parcel before compression is higher than that for zero axial temperature gradient and the temperature of a gas parcel before expansion is lower than that for zero axial temperature gradient. Hence,

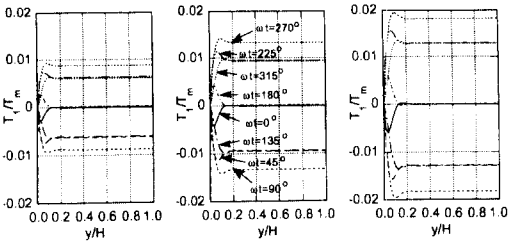

(L/s=30, Pr=0.7, γ=1.4, Ma=0.01, x/L=0.5, β=30)

Fig. 5 First-order temperature profiles for several $(dT_m/dx)/(T_m/L)$

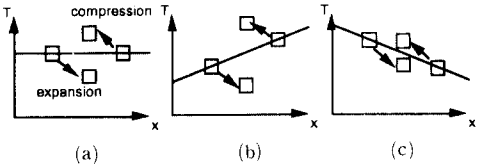

Fig. 6 Temperature variation of gas parcels

the temperature of a gas parcel after compression for positive axial temperature gradient is higher than that for zero axial temperature gradient and the temperature of a gas parcel after expansion is lower than that for zero axial temperature gradient. So when axial temperature gradient is positive, the temperature fluctuation at a location becomes larger as the magnitude of axial temperature gradient increases. But when axial temperature gradient is negative, the temperature fluctuation at a location becomes smaller as the magnitude of axial temperature gradient increases as shown in Fig. 6(c).

3.2 Steady second-order axial velocity

The steady component of the second-order axial velocity profiles at $x=L/2$ are shown in Fig. 7 for several values of β when $dT_m/dx=0$. For large β(e. g., $\beta=30$, 100) the gas in the core region flows from the closed end to the piston and the gas in the near-wall region flows from the piston to the cylinder head, which is consistent with the large scale streaming observation made by Lee et al.(1993). As β increases, the peak velocity near the wall increases, and the location of the peak velocity moves closer to the wall. For

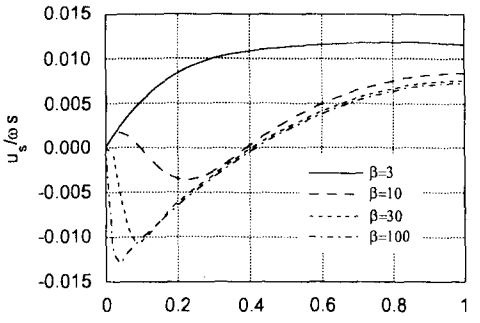

(L/s=30, Pr=0.7, γ=1.4, Ma=0.01, x/L=0.5)

Fig. 7 Steady second-order axial velocity profiles for $(dT_m/dx)/(T_m/L)=0$

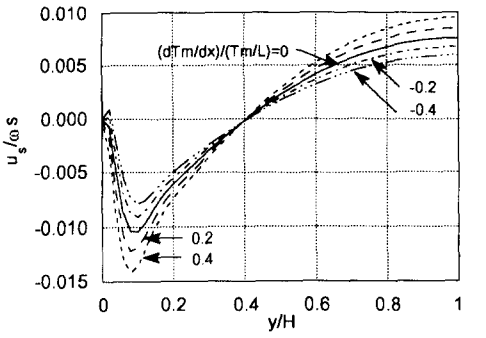

(L/s=30, Pr=0.7, γ=1.4, Ma=0.01, x/L=0.5, β=30)

Fig. 8 Steady second-order axial velocity profiles for several $(dT_m/dx)/(T_m/L)$

$\beta=10$ another flow reversal occurs near the wall. In the near-wall region and the center region, fluid flows from the closed end to the piston direction. In the intermediate region the fluid flows from the piston to the closed end. The parabolic shape of u_s for $\beta=3$ shows the same characteristics of leading terms of u_s for the case of $\beta \ll 1$ and $Pr<1$ in a long tube(Thomann, 1976). The velocity profile for $\beta=10$ appears to be a transitional velocity profile from the parabolic shape for small β to the flow reversal velocity profiles for large β. The mass flow through any cross section by the steady flow, $\rho_0 u_s$, is compensated by the net mass flow by the oscillating part of the flow, $<\rho_1 u_1>$, so that time-averaged mass flow through any cross section is zero.(see Eq. (30))

Fig. 8 shows that the magnitude of u_s for fixed β increases as dT_m/dx increases. Steady vorticity generation equation can be derived from Navier-Stokes equation as follows(Jeong, 1991).

$$\nabla^2 \vec{\omega}_s = \frac{1}{\mu}\left[< \rho_1 \frac{\partial \vec{\omega}_1}{\partial t} > + < \nabla \rho_1 \times \frac{\partial \vec{v}_1}{\partial t} > + < \rho_0 \nabla \times (\vec{v}_1 \bullet \nabla \vec{v}_1) > \right] \quad (33)$$

The first term on the right-hand side represents the steady vorticity generation due to density variation and unsteady rotational first-order velocity. The second term represents steady vorticity generation by the density gradient and unsteady first order velocity, and the third term represents the vorticity generation of incompressible viscous flow. The generation of steady rotational flow in fluids and gases traversed by sound waves is a well-established experimental fact(Westervelt, 1953). Theoretical studies of Rayleigh(1945) and Schlichting(1979) showed the existence of the streaming phenomena due to the interaction between inertia and viscosity neglecting heat conduction, and Jeong and Smith(1992a) showed that there exists a secondary flow due to all three mechanisms listed above for zero axial temperature gradient of the wall. Although they are not shown in this paper, the magnitudes of first-order velocities u_1 and v_1 increase slightly as axial temperature gradient increases. But the effects of axial temperature gradient on first-order velocities are not as large as that on the first-order temperature T_1 as shown in Fig. 5. As dT_m/dx increases the amplitude of density fluctuation and the density gradient in thermal boundary layer increase since the amplitude of the first-order temperature fluctuation increases as shown in Fig. 5. Hence, the magnitudes of the first and second terms on the right hand side of Eq. (33) increase as dT_m/dx increases, which results in the increase of the magnitude of u_s.

3.3 Steady second-order temperature

In Fig. 9 steady second-order temperature profiles at $x=L/2$ are shown for several values of β assuming $dT_m/dx=0$. T_s in Fig. 9 has the same

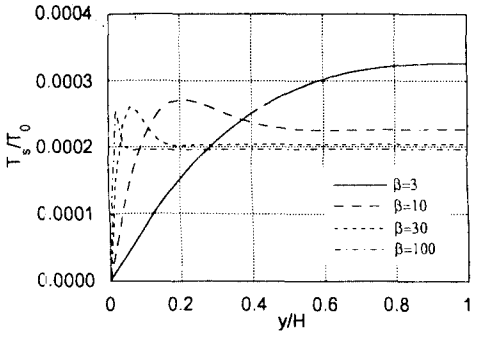

(L/s=30, Pr=0.7, γ=1.4, Ma=0.01, x/L=0.5)

Fig. 9 Steady second-order temperature profiles for $(dT_m/dx)/(T_m/L)=0$

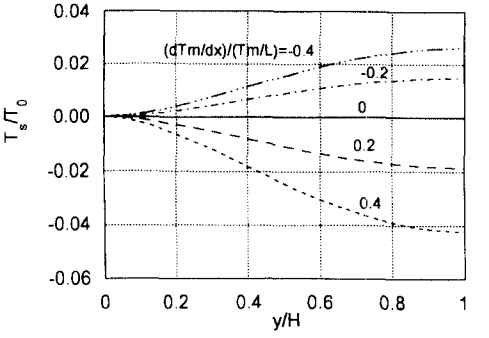

(L/s=30, Pr=0.7, γ=1.4, Ma=0.01, x/L=0.5, β=30)

Fig. 10 Steady second-order temperature profiles for several $(dT_m/dx)/(T_m/L)$

shape as those in Fig. 3 of Jeong and Smith(1992a) but the magnitudes are slightly different since the terms of order of $1/\beta$, which are neglected in Eq. (32) of Jeong and Smith, are included in Eq. (32). The positive temperature gradient at the wall indicates that net heat is always transferred from the gas to the wall. This shows how the net work done by the piston on the gas is removed from the gas to the wall as heat for the gas to maintain a cyclic steady state when $dT_m/dx=0$. Fig. 9 also shows that the mean temperature of the gas is higher than the wall temperature when $dT_m/dx=0$. For $\beta=3$ the temperature profile has a parabolic shape and has no peak point. But the temperature profiles for $\beta=10$, 30 and 100 have peaks near the wall. Associated with the oscillating first-order velocity component normal to the wall, net energy is transferred in the direction normal to the wall by mechanical energy flux due to the phase shift between p_1 and v_1. The time-average of $p_1 v_1$ acts like a heat source in time-averaged energy balance and is responsible for the existence of the peak points. The peak points clearly show that energy is transferred in the direction normal to the wall not only by heat conduction but also by mechanical energy flux.

Effect of axial temperature gradient on the steady second-order temperature is shown in Fig. 10. When dT_m/dx is positive, the mean temperature of the gas is lower than the wall temperature. When dT_m/dx is negative, the mean temperature of the gas is higher than the wall temperature. As the magnitude of dT_m/dx increases, the temperature difference between the gas and the wall increases. These phenomena can be understood by examining the time-averaged second-order energy equation.

$$\alpha_0 \frac{\partial^2 T_s}{\partial y^2} = \frac{\partial}{\partial x} < u_1 T_1 > + \frac{\partial}{\partial y} < v_1 T_1 > + \frac{\mu}{\rho_0 C_p} < u_1 \frac{\partial^2 u_1}{\partial y^2} > + \frac{\mu}{\rho_0 C_p} < \left(\frac{\partial u_1}{\partial y} \right)^2 > + < \frac{\rho_1}{\rho_0} u_1 > \frac{dT_m}{dx} + u_s \frac{dT_m}{dx} \tag{34}$$

As shown in Fig. 7 and 8 the gas outside boundary layer flows from the closed end to the piston for large β. When $dT_m/dx=0$ the second-order steady flow u_s does not contribute to the steady second-order temperature. When $dT_m/dx>0$ the fluid particles outside the boundary layer move steadily from the colder closed end side to the hotter piston side. Hence, the mean temperature of the gas is lowered as dT_m/dx increases as shown in Fig. 10. But, when $dT_m/dx<0$ the fluid particles outside the boundary layer move steadily from the hotter closed end side to the colder piston side. Hence, the mean temperature of the gas gets hotter as the magnitude of dT_m/dx increases.

3.4 Hysteresis loss and heat pumping

Hysteresis loss, which is defined as the net work

done by the piston on the gas during a cycle, is calculated from the cyclic integral of the piston pressure and volume change. Since the volume variation of the system is purely sinusoidal, only the first harmonic component of the pressure is responsible for hysteresis loss. From Eq. (23) the nondimensional hysteresis loss is given as:

$$(Loss)_{nd}=\frac{-\frac{1}{\tau}\int_0^{\tau} p_1(x=L+s\sin\omega t)\frac{dV}{dt}dt}{p_0 V_0/\tau}$$
$$=-\Re\left[\frac{i\pi\gamma}{D(\beta)}\frac{s^2}{L}\frac{\lambda_i\cos(\lambda_i L)+\lambda_r\sin(\lambda_i L)}{\sin(\lambda_i L)}\frac{1}{\{1-\tanh[(1+i)\beta]/(1+i)\beta\}}\right] \tag{35}$$

where $\Re$ denotes the real part of a complex number.

In Fig. 11 predictions of nondimensional hysteresis loss are shown for several axial temperature gradients. Hysteresis loss is low for small and large values of β, but significant for intermediate values of β. Small β and large β correspond to isothermal and adiabatic processes, respectively. The relation between hysteresis loss and β when $dT_m/dx=0$ was already shown by Lee(1983), Kornhauser and Smith(1988a) and Jeong and Smith(1992a). Positive hysteresis loss means that net work is done by the piston on the gas. The work is dissipated as heat mainly by heat conduction and transferred into the wall as shown in Fig. 9. Hysteresis loss for $dT_m/dx=0.3$ shows same trend as that of $dT_m/dx=0$, but the magnitude is larger than that of $dT_m/dx=0$. When dT_m/dx is negative($dT_m/dx=-0.3$) hysteresis loss is still positive, but the magnitude is smaller than that of $dT_m/dx=0$.

To understand the mechanism of surface heat pumping the heat transfer from the gas to the wall during a cycle is calculated from the time-averaged second-order energy Eq. (34). Integrating Eq. (34) from $y=0$ to $y=H$ gives

$$-\frac{k}{\rho_0 C_p}\frac{\partial T_s}{\partial y}\bigg|_{y=0}=\frac{\partial}{\partial x}\int_0^H <u_1 T_1>dy+\frac{\mu}{\rho_0 C_p}\int_0^H <u_1\frac{\partial^2 u_1}{\partial y^2}>dy+\frac{\mu}{\rho_0 C_p}\int_0^H <\left(\frac{\partial u_1}{\partial y}\right)^2>dy$$
$$+\frac{1}{\rho_0}\frac{dT_m}{dx}\int_0^H <\rho_1 u_1>dy+\frac{dT_m}{dx}\int_0^H u_s dy \tag{36}$$

The second and third terms on the right hand side of Eq. (36) disappear when integrated by part due to the boundary conditions $u_1=0$ at $y=0$ and $\partial u_1/\partial y=0$ at $y=H$. The fourth and fifth terms on the right hand side of the equation also disappear due to the fact that time-averaged mass flow across any cross-section is zero(see Eq. (30)).

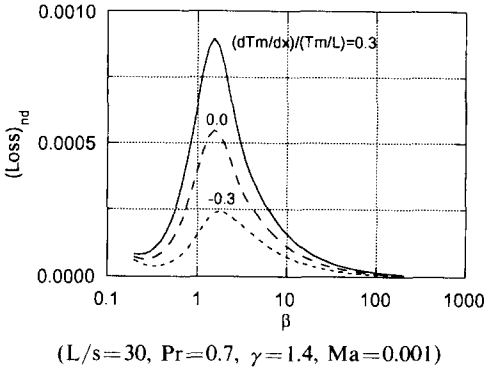

(L/s=30, Pr=0.7, γ=1.4, Ma=0.001)

Fig. 11 Nondimensional hysteresis loss

Finally, we can get

$$q_s=-\frac{\partial}{\partial x}\int_0^H \rho_0 C_p <u_1 T_1>dy \tag{37}$$

where

$$q_s=k\frac{\partial T_s}{\partial y}\bigg|_{y=0} \tag{38}$$

q_s represents the steady heat flux from the gas to the wall, and the term on the right hand side of Eq. (37) can be interpreted as 'thermal streaming' (Rott, 1974). Steady heat flux from the gas to the wall is obtained by substituting the expressions of u_1 and T_1 in Eqs. (19) and (21) into Eq. (37) and numerically integrating Eq. (37).

Fig. 12 shows q_s along the wall for $\beta=2$. When dT_m/dx is zero or positive heat is transferred from the gas to the wall in cyclic-average sense. q_s is almost constant along the wall when $dT_m/dx=0$, but q_s increases as x increases when $dT_m/dx=0.3$. When $dT_m/dx=-0.3$, q_s is negative in the

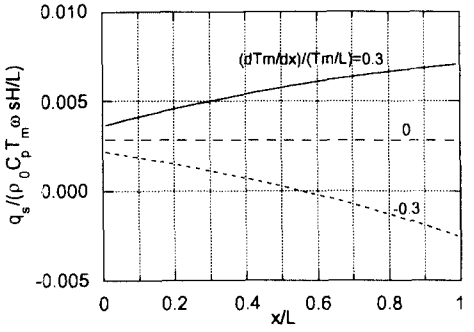

(L/s=30, Pr=0.7, γ=1.4, Ma=0.001, β=2)

Fig. 12 Cyclic-averaged heat flux to the wall

region near piston and positive in the region near closed end. In other words, the wall near piston gives net heat to the gas and the wall near closed end receives net heat from the gas. Thus, heat is pumped from the colder wall near piston to the hotter wall near closed end. This phenomenon is called as 'surface heat pumping' and is the operating mechanism of pulse-tube refrigerator(Gifford and Longsworth, 1963 and 1966). When $dT_m/dx = -0.3$ the gas in the cylinder-piston apparatus in Fig. 1 gives more heat to the wall than it receives from the wall is cyclic-average sense. The difference between the heat received from the wall and that given to the wall in balanced by the net work done by the piston. So, the gas in Fig. 1 receives net work from the piston and transfers net heat from the colder region of the wall to the hotter region of the wall.

3.5 Complex Nusselt number for oscillating pressure and flow

Complex Nusselt number was introduced to take into account the phase shift between the heat flux at the wall and the wall-bulk gas temperature difference for conditions of oscillating pressure(Lee, 1983), incompressible oscillating flow(Gedeon, 1986), and oscillating pressure and flow(Kornhauser and Smith, 1989).

From Eq. (21) the expressions of heat flux at the wall and bulk temperature of the gas can be obtained. Using these expressions we can get the following relation.

$$Nu_c=\frac{H}{k}\frac{\dot{q}_w}{(T_w-T_{bulk})}$$
$$=(1+i)\beta\sqrt{Pr}\,\frac{\tanh[(1+i)\beta\sqrt{Pr}]-\zeta\left\{\frac{\sqrt{Pr}}{Pr-1}\tanh[(1+i)\beta]-\frac{1}{Pr-1}\tanh[(1+i)\beta\sqrt{Pr}]\right\}}{1-\frac{\tanh[(1+i)\beta\sqrt{Pr}]}{(1+i)\beta\sqrt{Pr}}-\zeta\left\{1-\frac{Pr}{Pr-1}\frac{\tanh[(1+i)\beta]}{(1+i)\beta}+\frac{1}{Pr-1}\frac{\tanh[(1+i)\beta\sqrt{Pr}]}{(1+i)\beta\sqrt{Pr}}\right\}} \tag{39}$$

where

$$\zeta=\frac{C_p}{\omega^2}\frac{dT_m}{dx}\frac{(dp_1/dx)}{p_1}=\frac{C_p}{\omega^2}\frac{dT_m}{dx}\frac{|(dp_1/dx)|}{|p_1|}e^{i\phi} \tag{40}$$

Here ϕ denotes the phase angle between p_1 and dp_1/dx. $|p_1|$ and $|dp_1/dx|$ denote the amplitudes of the fluctuations of pressure and axial pressure gradient, respectively. Examination of Eqs. (19) and (21) shows that ζ is the ratio of the temperature variation of the gas due to oscillating flow and axial temperature gradient to that caused by oscillating pressure. Complex Nusselt number developed for oscillating pressure and oscillating plug flow(Kornhauser, 1989) is the same as that of oscillating pressure(Lee, 1983). But Eq. (39) shows that complex Nusselt number for oscillating pressure and flow condition is different from that of oscillating pressure condition if we take into account of viscosity effect. It $\zeta=0$, the expression of Eq. (39) is identical to that of Lee(1983) and Kornhauser(1989).

Fig. 13 shows the real and imaginary parts of complex Nusselt number for several values of ζ. For small β the real part of Nu_c is almost constant and the imaginary part is very small, but for large β the real and imaginary parts for same ζ are nearly same. This shows that when β is small the heat flux at the wall is in phase with the wall-to-gas temperature difference as in steady state heat transfer since small β means low piston

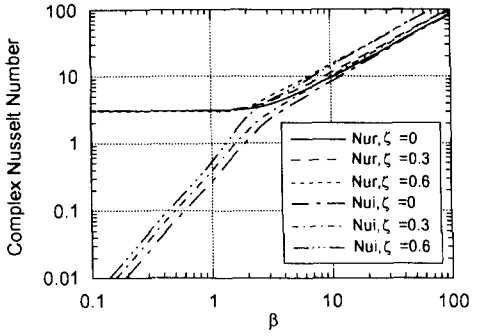

Fig. 13 Complex Nusselt number for oscillating pressure and flow conditions

frequency, but when β is large the heat flux at the wall advances the wall-to-gas temperature difference by 45° since piston frequency is high. For small β the real part of Nu_c does not vary much as ζ varies, but the imaginary part increases as ζ increases. For large values of β the real and imaginary parts increase as ζ increases. Since the expressions of u_1 and T_1(Eqs. (19) and (21)), from which Eq. (39) is derived, are derived for arbitrary oscillating p_1 and dp_1/dx, the complex Nusselt number of Eq. (39) can be used for any gas confined by two parallel plates and can be applied for all values of β.

4. Conclusion

The coupled heat and momentum transfer problem in a closed-volume piston-cylinder apparatus with a constant axial wall temperature gradient is solved analytically. The results show that there exists a steady component of heat flux from the gas to the wall and that there exists a steady circulating flow. Effects of axial temperature gradient on the steady second-order axial velocity and temperature are shown. By calculating the steady heat flux from the gas to the wall, the mechanism of surface heat pumping is explained analytically. A new heat transfer both relation under conditions of both oscillating pressure and oscillating flow, which can be used in one-dimensional models for both design and analysis of reciprocating machinery such as Stirling machines and pulse-tube refrigerators, is proposed.

Acknowledgement

This work is supported by Hong Ik University research fund.

References

Annand, W. J. D. and Pinfold, D., 1980, "Heat Transfer in the Cylinders of a Motored Reciprocating Engines," *SAE Paper* 800457, Society of Automotive Engineers.

Faulkner, H. B. and Smith, J. L., Jr., 1983, "Instantaneous Heat Transfer During Compression and Expansion in Reciprocating Gas Handling Machinery," *Proceedings of the 18th Intersociety Energy Conversion Engineering Conference*, pp. 724~730.

Faulkner, H. B. and Smith, J. L., Jr., 1984, "The T-S Diagram as an Indicator of Instantaneous Wall-to-Gas Heat Transfer Driven by a Quasi-Static Periodic Gas Pressure," *ASME Paper* No. 84-WA/HT-45, American Society of Mechanical Engineers.

Gedeon, D., 1986, "Mean-Parameter Modeling of Oscillating Flow," *Journal of Heat Transfer,* Vol. 108, No. 3, pp. 513~518.

Gifford, W. E. and Longsworth, R. C., 1963, "Pulse-Tube Refrigeration," *ASME Paper* No. 63-WA-290, American Society of Mechanical Engineers.

Gifford, W. E. and Longsworth, R. C., 1966, "Surface Heat Pumping," *Advances in Cryogenic Engineering*, Vol. 11, pp. 171~179.

Jeong, E. S., 1991, "Heat Transfer with Oscillating Pressure in Reciprocating Machinery," Ph. D. Thesis, Dept. of Mech. Eng., Massachusetts Institute of Technology, Cambridge, MA.

Jeong, E. S. and Smith, J. L., Jr., 1992a, "Secondary Flow in Reciprocating Machinery," *Proceedings of the ASME National Heat Transfer Conference,* Vol. 24, pp. 97~104.

Jeong, E. S. and Smith, J. L., Jr., 1992b, "An Analytic Model of Heat Transfer with Oscillating Pressure," *Proceedings of the ASME National Heat Transfer Conference*, Vol. 24, pp. 105~113.

Kornhauser, A. A., 1989, "Gas-Wall Heat Transfer During Compression and Expansion," Sc. D. Thesis, Dept. of Mech. Eng., Massachusetts Institute of Technology, Cambridge, MA.

Kornhauser, A. A. and Smith J. L., Jr., 1988a, "Integration of Analysis and Experiment for Stirling Cycle Processes. Part 1-Gas Spring Hysteresis Loss," *Proceedings of the 2nd DOE/ORNL Heat Pump Conference,* DOE/ORNL CONF-8804100, pp. 203~208.

Kornhauser, A. A. and Smith J. L., Jr., 1988b, "Application of a Complex Nusselt Number to Heat Transfer During Compression and Expansion," *On Flows in Internal Combustion Engines-IV,* American Society of Mechanical Engineers, pp. 1~8.

Kornhauser, A. A. and Smith J. L., Jr., 1989, "Heat Transfer with Oscillating Pressure and Oscillating Flow," *Proceedings of the 24th Intersociety Energy Conversion Engineering Conference,* Vol. 5, pp. 2347~2353.

Lee, J. M., Kittel, P., Timmerhaus, K. D. and Radebaugh, R., 1993, "Flow Patterns Intrinsic to the Pulse Tube Refrigerator," *Proceedings of the 7th International Cryocooler Conference,* pp. 125~139.

Lee, K. P., 1983, "A Simplistic Model of Cyclic Heat Transfer Phenomena in Closed Spaces," *Proceedings of the 18th Intersociety Energy Conversion Engineering Conference,* pp. 720~723.

Merkli, P. and Thomann, H., 1975, "Thermoacoustic Effects in a Resonance Tube," *J. Fluid Mech.*, Vol. 70, pp. 161~177.

Pfriem, H., 1943, "Periodic Heat Transfer at Small Pressure Fluctuations," *NACA-TM-1048,* National Advisory Committee for Aeronautics, (Translated from *Forschung auf dem Gebiete des Ingenierwesens,* Vol. 11, No. 2, 1940, pp. 67~75).

Rayleigh, Lord, 1945, *The Theory of Sound,* Vol. 2, Dover Publications, pp. 340~342.

Rott, N., 1974, "The Heating Effect Connected with Non-Linear Oscillations in a Resonance Tube," *Journal of Applied Mathermatics and Physics*, Vol. 25, pp. 619~634.

Schlichting, H., 1979, *Boundary Layer Theory,* McGraw-Hill, pp. 428~432, p. 463, p. 690.

Swift, G. W., 1988, "Thermoacoustic Engines," *Journal of Acoustical Society of America,* Vol. 84, No. 4, pp. 1145~1180.

Tew, R. C., Jr., 1987, "Overview of Heat Transfer and Fluid Flow Problem Areas in Stirling Engine Modeling," *Fluid Flow and Heat Transfer in Reciprocating Machinery,* American Society of Mechanical Engineers, pp. 77~88.

Thomann, H., 1976, "Acoustical Streaming and Thermal Effects in Pipe Flow with High Viscosity," *Journal of Applied Mathematics and Physics,* Vol. 27, pp. 709~715.

Westervelt, P. J., 1953, "The Theory of Steady Rotational Flow Generated by a Sound Field," *Journal of Acoustical Society of America,* Vol. 25, No. 1, pp. 60~67.